Superconducting Bearing Design for Outer Rotor Flywheel Using Lumped Parameter Techniques

Clay Hearn[a], Siddharth Pratap[a], Dongmei Chen[b], Raul Longoria[b]

[a] University of Texas at Austin, Center for Electromechanics, Austin, Texas, USA
hearn@cem.utexas.edu
[b] University of Texas at Austin, Department of Mechanical Engineering, Austin, Texas, USA

***Abstract*— This paper describes the application of lumped parameter modeling techniques to designing high temperature superconducting bearings for outer-rotor flywheel energy storage systems. The lumped parameter models decrease computational time by 99% compared to Finite Element Analysis (FEM) without compromising fidelity needed to capture the non-linear and hysteretic force-displacement behavior between a levitated permanent magnet and bulk superconductor. The techniques formulated can be used to quickly evaluate lifting capacity and translational stiffness for a superconducting bearing design. The validity of the modeling approach has been verified by comparing results from FEM studies and experimental tests.**

I. INTRODUCTION

Flywheel energy storage has become an attractive storage technology for specific grid utility services where high power density and cycle rates are required. At the moment, potential applications for flywheel energy storage lie in shorter term storage applications below 20 minutes, such as voltage/frequency regulation services and power smoothing [1, 2].

A limitation to increase efficient storage times of flywheels from minutes to hours and days has been due to inherent storage losses, or leakage [3]. This leakage is primarily attributed to aerodynamic windage and losses through the bearings. Windage losses can be minimized by operating under hard vacuums, typically under 1 Torr [4], whereas magnetic bearings are currently employed to minimize bearing losses. Although magnetic bearings significantly reduce losses compare to contact style bearings, these bearings still suffer from losses due to eddy currents and magnetic hysteresis, effects that can lead to loss rates up to 2%-5% per hour [5, 6]. Optimization of bearing designs can drop the loss rate down to 0.5% per hour [7].

High temperature superconducting (HTSC) bearings can lead to further reduce loss rates associated with bearings. Flywheel systems with HTSC bearings have been demonstrated at very low loss rates of 0.1% per hour [5], which translates into a free spin down time constant of 1000 hrs. HTSC bearings are also passive and require little to no additional control structure for stable operation. The basic construction of an HTSC bearing for a flywheel application consists of the stable levitation of a permanent magnet pinned to a bed of bulk high temperature superconductors.

This work was supported by Stanford University through the Global Climate and Energy Project (GCEP).

Compared to designing active magnetic bearings, where a magnetic circuit can be defined to estimate air gap fluxes and potential bearing stiffness, there are very few low order methods for describing the non-linear and hysteretic behavior between a levitated permanent magnet pinned to a bulk superconductor. The most simple model for this interaction is the advanced mirror image method [8, 9]. This method models the permanent magnet as a dipole interacting with a frozen image and diamagnetic mirror image. Although this modeling technique can be readily implemented, the model assumes the bulk superconductors are perfect conductors and ignores the highly non-linear losses which limit induced currents to the critical current density. High level finite element methods (FEM) can capture these effects [10] but, while they are the most accurate methods to use, they are computationally intensive. For the initial design stage of a flywheel with high temperature superconducting bearings, a lower order modeling method is desired to estimate lifting capacity and bearing stiffness. This is especially necessary for outer-rotor flywheel designs where many design iterations may be required to balance magnet banding strength and mass loading against the supporting composite bandings.

The authors of this paper have presented methodologies for lumped parameter models in an axisymmetric [11] and 3D frame [12] to describe the dynamic interaction between a levitated permanent magnet pinned to a bulk high temperature superconductor. Both models in their respective publications were confirmed against FEM analysis and experimental tests. Compared to FEM methods, the lumped parameter models reduce computational time by up to 99%, without sacrificing the nonlinear and hysteretic system dynamics. This paper describes how these techniques can be used to assess lifting capacity and bearing stiffness for HTSC bearing designs of outer rotor flywheel systems.

II. BEARING TOPOLOGY AND MODEL DEVELOPMENT

Lumped parameter modeling is a technique that subdivides a system into discrete elements which can be represented by a select, finite, number of states. The state space formulation of these models is represented by a set of ordinary differential equations (ODEs) that can be quickly solved through numerical integration. For modeling bearing systems that

utilize the stable levitation of permanent magnets over bulk high temperature superconductors, the lumped parameter models sub-divide the superconductors into pre-defined elements to estimate bulk average current flow, which is the local state. For the axisymmetric case [11], the superconducting plate is sub-divided into nested concentric ring elements which are concentrically constrained to the fields produced by the permanent magnet. For mechanical considerations, this model formulation is useful for estimating the bearing lifting capacity and the dynamic axial stiffness. In the 3D formulation [12], the bulk superconducting region is subdivided into overlapping disc elements which allow the model to simulate non-circular surface currents that will be induced due to translational movement of the magnet. A representation of a single permanent magnet levitating over a bulk HTSC disc is shown in Figure 1 for both respective model formulations.

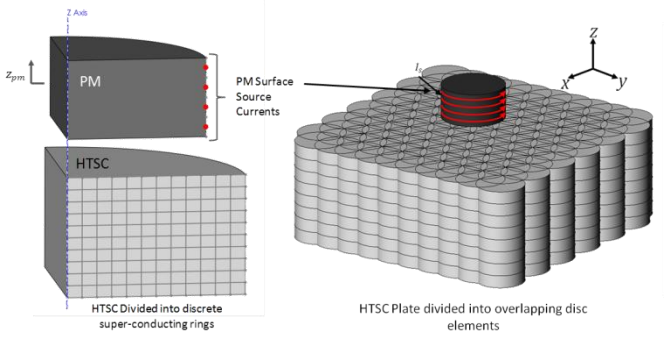

Figure 1: Left: Permanent magnet levitating over a bulk HTSC disc modeled as concentric ring elements for the axisymmetric model. Right: Permanent magnet levitating over a bulk HTSC block modeled as overlapping disc elements for the 3D model.

Utilizing Faraday's law of induction, a set of differential equations (1) can be developed to estimate the induced element currents, I_n, in the respective lumped parameter models. The spatial gradients of the magnetic fields, ϕ, produced by the permanent magnet array link the component velocity, v, of the magnet array to the electromotive force induced on each element. From bond graph terminology [13], these spatial gradients can be identified as gyrator moduli, which represent ideal power conversions between the magnetic and mechanical elements within the system. These moduli are also used to calculate the resultant force on the magnet array due to movement (2). The inductance matrix, **L**, is a symmetric matrix that includes all self and mutual inductance values for the superconducting elements within the system.

$$\begin{bmatrix} \frac{dI_1}{dt} \\ \frac{dI_2}{dt} \\ \vdots \\ \frac{dI_N}{dt} \end{bmatrix} = -\boldsymbol{L}^{-1}\left[\begin{bmatrix} e_1 \\ e_2 \\ \vdots \\ e_N \end{bmatrix} + \begin{bmatrix} \frac{d\phi_1}{dx} \\ \frac{d\phi_2}{dx} \\ \vdots \\ \frac{d\phi_N}{dx} \end{bmatrix} v_x + \begin{bmatrix} \frac{d\phi_1}{dy} \\ \frac{d\phi_2}{dy} \\ \vdots \\ \frac{d\phi_N}{dy} \end{bmatrix} v_y + \begin{bmatrix} \frac{d\phi_1}{dz} \\ \frac{d\phi_2}{dz} \\ \vdots \\ \frac{d\phi_N}{dz} \end{bmatrix} v_z\right] \quad (1)$$

$$\boldsymbol{F} = \left(\sum_{j=1}^{N} -\frac{d\phi_j}{dx} I_j\right)\hat{\boldsymbol{\imath}} + \left(\sum_{j=1}^{N} -\frac{d\phi_j}{dy} I_j\right)\hat{\boldsymbol{\jmath}} + \left(\sum_{j=1}^{N} -\frac{d\phi_j}{dz} I_j\right)\hat{\boldsymbol{k}} \quad (2)$$

For high temperature superconductors, once the upper critical magnetic field is exceeded, the material loses the property of superconductivity and becomes resistive. At this point, the current flow within the material is saturated at the critical current density, J_c. The model formulation in (1) includes power-law based resistance components, e_n, to model the rapid rise in resistivity once the critical current density is exceeded. The power law method has been effectively used in FEM studies to model these loses and saturation effects [10].

To estimate the magnetic flux produced by the permanent magnet that penetrates each ring or disc element of the respective axisymmetric or 3D models, the magnet is modeled by discrete current loops on the exterior surface which produce an equivalent magnetic field strength. For each surface current loop, I_s, the magnetic vector potential, $\boldsymbol{A}$, can be calculated at any point with respect to the loop by using a formulation of the Biot-Savart Law, as presented by Smythe [14]. From Figure 3, Smythe's formulation of the vector potential is shown in (3), where K and E are elliptical integrals of the first and second kind, with modulus k_{si} (4).

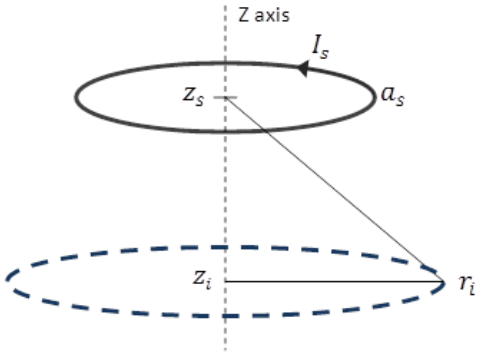

Figure 2: Schematic of fixed source current loop (on magnet surface) with current, I_s, radius, a_s, and axial position z_s, to a passive filament ring element (within superconducting element) with radius, r_i and axial position z_i.

$$\boldsymbol{A} = \frac{\mu_0 I_s}{\pi k_{si}}\left(\frac{a_s}{r_i}\right)^{\frac{1}{2}}\left(\left(1-\frac{1}{2}k_{si}^2\right)K(k_{si}) - E(k_{si})\right) \quad (3)$$

$$k_{si} = \sqrt{\frac{4a_s r_i}{(a_s + r_i)^2 + (z_i - z_s)^2}} \quad (4)$$

From the magnetic vector potentials, Stokes Theorem (5) can be used to calculate the magnetic flux through any surface or closed path. From here, the Leibnitz rule is used to calculate the spatial derivatives (where q_i is x_i, y_i, or z_i respectively) of the magnetic flux (6) through a closed circular loop of a superconducting element to calculate the gyrator moduli used in (1).

$$\phi = \iint \nabla \times \boldsymbol{A} \cdot d\boldsymbol{S} = \oint \boldsymbol{A} \cdot d\boldsymbol{l} \tag{5}$$

$$\frac{d\phi_{ij}}{dq_i} = \int_0^{2\pi} \frac{\partial}{\partial q_i}\left[\phi_{ij}(q,\theta)\right] d\theta \tag{6}$$

The respective papers on axisymmetric and 3D model development, [11] and [12], give detailed techniques for calculating these moduli based on the specific geometric constraints for each model.

III. Application to Bearing Design

The lumped parameter models may be applied during the initial design phase of a superconducting bearing for an outer rotor flywheel to determine lifting capability and translational stiffness. The bearings should be sized to support the weight of the flywheel, and axial and translational stiffness values must be assessed to ensure no instabilities occur during operation. An outer rotor flywheel consists of a set of high strength composite rings that are levitated and spun to store energy in the kinetic form. Rotor side bearing and motor-generator elements are typically located on the ID (inner diameter) bore of the composite bandings. This design topology maximizes energy stored to mass ratios for the final flywheel system. For the superconducting bearings, the size and layout of the rotor side permanent magnets must be optimized to limit mass loading of the surrounding composite bandings during operation.

A topology for a 25 kWh outer-rotor flywheel with end face HTSC bearings is shown in Figure 3 [6]. This proposed flywheel is a notional design for utility scale load-leveling that was developed to demonstrate the lumped parameter modeling technique for a complete bearing set. An array of permanent magnets sits within the end-faces of the outer rotor composite bandings on either side to stably levitate the flywheel and allow near lossless rotation about the spin axis. Typically, the permanent magnets are arranged in a Halbach or alternating pole pair arrangement to increase field gradients and overall stiffness [15, 16]. The bearing arrangement may also be located on the ID bore of the composite bandings in a journal bearing configuration [17]. Flywheel dimensions, mass, and operating speed are shown in Table I.

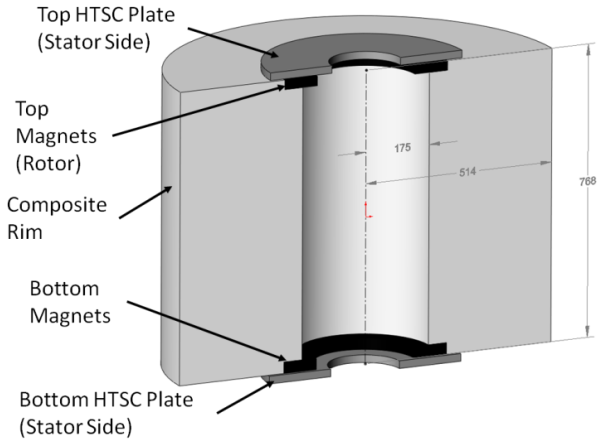

Figure 3. Notional 25 kWh flywheel rotor design using HTSC face bearings for levitation.

Table 1: Flywheel dimensions for bearing analysis

Inner Radius	Outer Radius	Length	Mass	Delivered Energy	Speed
0.175 m	0.514 m	0.768 m	878 kg	25 kWh	13,000 RPM

IV. Axisymmetric Analysis

The initial design analysis utilizes the axisymmetric modeling methodology to determine the bearing lifting capability. The bearings must support the full weight of the flywheel assuming that the flywheel is vertically oriented. The equations for axisymmetric model are solved with a fixed step, 4th order Runge-Kutta solver, which improves computational time and allows optimization studies to be performed. For this analysis a parametric study was performed to optimize pole pair arrangement of the permanent magnets to maximize lifting force and vertical stiffness.

A schematic of one of the superconductor bearing sets is shown in Figure 4. For the axisymmetric model, the HTSC plate is sub-divided into 300 concentric superconducting ring elements assuming a critical current density of 12 kA/cm^2. The plate of bulk superconductors has an inner radius of 105 mm, outer radius of 265 mm, and an axial thickness of 15 mm. The corresponding permanent magnets, which are located on the end faces of the composite bandings, have an inner radius of 145mm, outer radius of 225mm and axial thickness of 30mm. The inner radius of the permanent magnet set, which is smaller than the inner radius of the bandings described in Table 1, would require additional support structure that would need to be considered in a structural analysis. The permanent magnets are assumed to have an equivalent surface current strength of 1030 kA/m. Discrete current loops, I_s, on the cylindrical faces of the permanent magnets are employed to generate the equivalent magnetic fields, as shown in the break-out image in Figure 4. When the flywheel is centered axially, there is a 2mm air gap between the permanent magnets and bulk superconductors on the top and bottom faces.

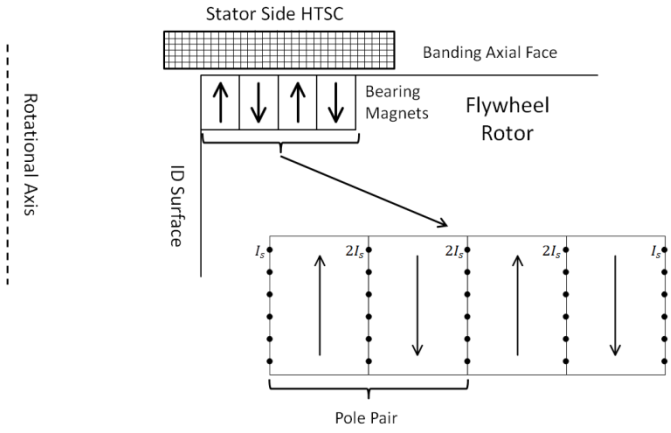

Figure 4: Schematic of pole pair arrangement for HTSC bearing.

An analysis using the axisymmetric modeling method evaluated the impact of pole pair arrangement of the permanent magnets for lifting capacity and axial stiffness. This analysis assumed 1, 2, and 3 alternating north-south pole pairs. Since the inner and outer radii of the permanent magnet

region was assumed locked for this study, increasing the pole pair count reduced the radial width of the permanent magnet elements. To determine potential lifting capacity and stiffness, the flywheel rotor is axially swept through available gap space. This movement occurs after cooling the bulk superconductors below critical and is necessary in order to induce currents within the bulk HTSC, that will provide the levitation force. The bearing superconductors are initially cooled with the flywheel positioned at $z_{fw} = +1.8mm$. The flywheel is then swept between $z_{fw} = +1.8mm$ and $z_{fw} = -1.8mm$ for 2 cycles over a time span of 60 seconds to determine the force displacement characteristic. This low rate of axial speed, v_z = 0.24 mm/s, to avoid inducing additional losses within the bulk superconductors.

This analysis generates a force-displacement profile for the HTSC bearing set where lifting capability and axial stiffness can be evaluated. Figure 5 presents the results for the 2 pole pair magnet arrangement, where the top graph shows the forces for the top and bottom bearing plates and the bottom graph shows the net axial bearing force. Through the movement cycle, there are 4 equilibrium points where the net bearing force equals the weight of the flywheel rotor. This analysis reveals a nonlinear hysteresis in the force-displacement plots that is due to the internal losses which result in trapped fields within the bulk superconductors.

Table 2 summarizes the study results and shows that 2 pole pairs is an optimal magnet arrangement for this design. Using 2 pole pairs maximizes the vertical stiffness of the bearing set and produces an equilibrium which is closest to center for the axial position of the flywheel rotor.

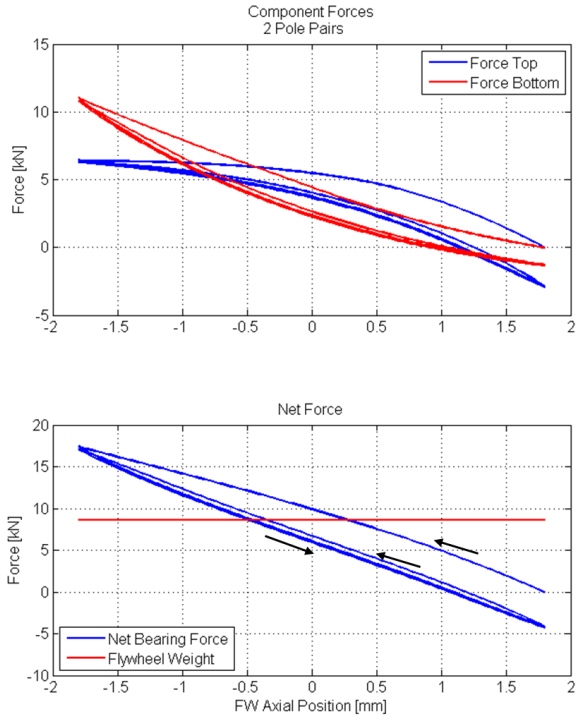

Figure 5: Force displacement curve of flywheel swept two times between +/- 1.8mm with 2 pole pairs.

Table 2: Summary of axisymmetric analysis

Pole Pairs	1	2	3
Magnet Width [mm]	40.0	20.0	13.3
Equilibrium [mm]	-0.912	-0.339	-0.707
Stiffness [kN/m]	3750	5500	5417

V. Translational Analysis

From the results of the axisymmetric analysis, the 3D lumped parameter modeling method [12] is used to estimate the translational bearing stiffness of the 2 pole pair bearing configuration. This method requires sub-dividing the superconducting region into individual, overlapping superconducting disc elements to estimate induced current flow. Compared to the axisymmetric method, the 3D model is more computationally intensive for calculating the field gradients per (6) since symmetry cannot be used. To improve model performance, these field gradients are calculated off-line and then stored in 3-D lookup tables for solving the main body of equations in (1).

In order to achieve accurate analysis results, the meshed overlapping disc elements for the superconducting plates must have diameters less than the interacting pole widths. This meshing requirement can significantly increase model order and calculation time. In order to reduce element count, the HTSC plate thickness is reduced to 5mm, which covers the penetration of induced currents per the axissymmetric analysis. The mesh for the transverse analysis uses 2 layers of overlapping disc elements, each with a diameter of 14mm. The layer closer to the interacting magnet had a thickness of 1 mm, while the second layer had the remaining thickness of 4mm. A total of 6,156 disc elements were used for each HTSC plate, as shown in Figure 6.

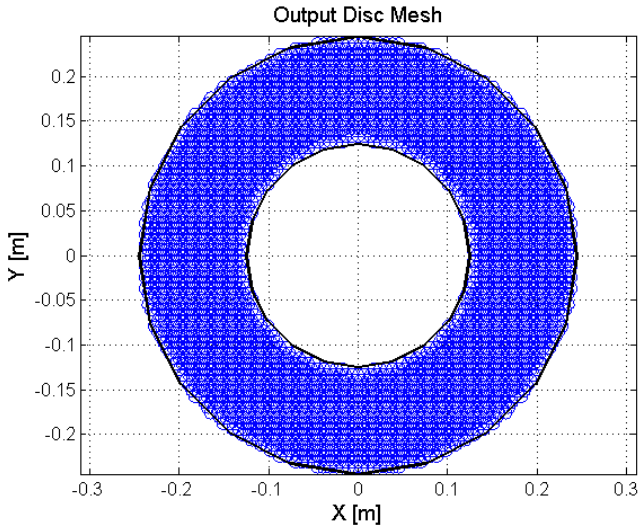

Figure 6: Disc element mesh for transverse analysis

The first step in performing the translational analysis with the 3D model is to re-perform the axial sweep and settle the model at the equilibrium position. This step is performed to estimate the induced currents and flywheel axial position at

equilibrium, which will be used as initial conditions for the transverse sweep simulation.

Once the initial conditions at equilibrium are determined, a controlled constant velocity sweep in the x direction is performed, similar to the vertical sweep performed in the axisymmetric analysis. For the translational analysis, the flywheel is swept between +/- 1 mm for 2 cycles over a time span of 30 seconds. Again, this model is solved with a 4th order Runge-Kutta using a time step of 2 ms. The results from the translational sweep analysis are shown in Figure 7. As the bearing is moved off-center, the induced currents within the HTSC plates produce a translational force in the x direction on the bearing to push it back to the original position. In addition to this translational force, an axial force is also generated on the permanent magnets in the z direction. These force components can be clearly identified in (2) where axial flux gradients, $\frac{d\phi_j}{dz}$, couple with induced currents. This repulsive axial force is a summation of a decrease in lifting capacity of the top plate and an increase of lifting capacity on the bottom plate.

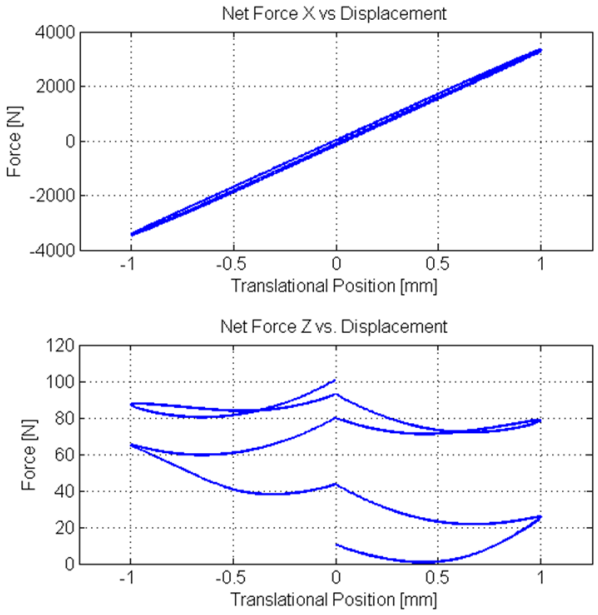

Figure 7: Bearing translational force versus translational movement

VI. Application Towards Rotor Dynamics

The results from this analysis can be applied to rotor dynamic analyses to identify rigid body modes. HTSC bearings typically have low stiffness values and will have to traverse one or two critical modes on initial spin up. Ideally, the flywheel should operate in a speed regime where no modes are present, but in order to reach operating speed it may run through a mode. It is necessary to determine the location of these modes during the design process to assess how they may affect operation. The bearing stiffness values for the top and bottom pairs are shown in Table 3.

Table 3: Axial, translational, and cross coupling bearing stiffness predicted from lumped parameter models.

	Top	Bottom
K_{zz}	1833 kN/m	3667 kN/m
K_{xx}	1770 kN/m	1610 kN/m
K_{xz}	-143 kN/m	158 kN/m

For a first pass analysis, a rigid body assumption can be used to estimate critical modes with respect to operating speeds. Linearized equations, presented by Schweitzer [18], were used with the respective translational stiffness values, K_{xx}, for the top and bottom bearing pairs. In this type of analysis, the gyroscopic coupling is the only variable that affects the resonance frequencies as a function of speed. From this analysis, a Campbell diagram can be produced which shows the critical resonance frequencies as a function of rotor speed, Figure 8.

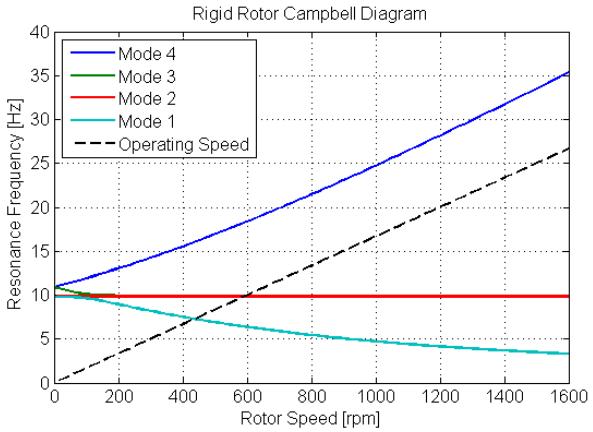

Figure 8: Rigid body vibration modes versus rotor speed and operational load line.

From the rigid body analysis for the 25 kWh outer rotor flywheel design, the flywheel will need to contend with crossing a single critical mode, Mode 2, at a speed of 600 rpm. Modes 1 and 3 are backward whirl modes that should not be excited since they are opposite the spin direction. Mode 2 is a forward whirl mode which can be excited by potential imbalances in the flywheel. Mode 4 is a conical whirl mode, but should not be excited during operation at any point since the polar to transverse inertia ratio is greater than 1 for the flywheel design.

The nominal operating speed of this notional flywheel design is between 6,500 and 13,000 rpm, which is significantly higher than the 2nd mode crossing, but to initially get the flywheel up to speed, this mode will need to be considered. Possible ways to get through this mode include the addition of copper rings to add damping to the system which will attenuate the effects of the mode. This method would induce a constant source of eddy current losses that will increase the overall bearing loss. Another method to transverse this mode is to add a set of active magnetic bearings which can be activated to change the radial stiffness and rigid body dynamics so that the flywheel passes through the mode. These supplemental active magnetic bearings should not be

designed using a permanent magnet bias design, as this would constantly induce losses during operation. Since this bearing should only be "activated" during a small portion of time when the flywheel is spinning up to operation speed, a bias field current could be used for bearing control to eliminate losses during nominal operation.

VII. Conclusions

The lumped parameter modeling method significantly improves calculation time over FEM analysis without ignoring internal losses within the bulk superconductors that limit maximum current density and produce the non-linear hysteretic force-displacement behavior. The equations are formulated in state-space as a set of ordinary differential equations that can be efficiently and deterministically solved using fixed step Runge-Kutta methods. The axisymmetric method is used to evaluate the axial stiffness and weight carrying capability for a proposed flywheel design. The 3D method is used to estimate the translational bearing stiffness, which will affect rotordynamics. Both of the methods presented in this paper can be incorporated into larger mechanical models to fully simulate flywheel dynamics.

The analysis presented in this paper is one of the first steps in a bearing design for an outer rotor composite flywheel. Along with bearing performance, the mechanical performance of the loaded composite rotor must be assessed. The addition of permanent magnets on the end faces of the composite rotor will cause additional mass loading of the surrounding composite bandings at speed. Iterative structural analyses will be required to determine the impact of this additional mass loading, and may require a redesign of the proposed magnet arrangement. The quick turn-around time afforded by the techniques presented will greatly aid such an iterative design analysis approach.

References

[1] P. Denholm, E. Ela, B. Kirby and M. Milligan, "The Role of Energy Storage with Renewable Electricity Generation," NREL/TP-6A2-47187, Golden, CO, January 2010.

[2] M. L. Lazarewicz and T. M. Ryan, "Integration of flywheel based energy storage for frequency regulation on deregulated markets," in Power and Energy Society General Meeting, July 2010.

[3] C. S. Hearn, M. C. Lewis, S. B. Pratap, R. E. Hebner, F. M. Uriate, D. Chen and R. G. Longoria, "Utilization of Optimal Control Law to Size Grid-Level Flywheel Energy Storage," IEEE Transactions on Sustainable Energy, vol. 4, no. 3, pp. 611-618, July 2013.

[4] M. M. Flynn, "A Methodology for Evaluating and Reducing Losses, Heating, and Operational Limitations of High-Speed Flywheel Batteries," Dissertation to The University of Texas at Austin, August 2003.

[5] M. Strasik, P. E. Johnson, A. C. Day, J. Mittleider, M. D. Higgins, J. Edwards, J. R. Schindler, K. E. McCrary, C. R. McIver, D. Carlson, J. F. Gonder and J. R. Hull, "Design, Fabrication, and Test of a 5-kWh/100-kW Flywheel Energy Storage Utilizing a High-Temperature Superconducting Bearing," IEEE Transactions on Applied Superconductivity, vol. 17, no. 2, pp. 2133-2137, June 2007.

[6] C.S. Hearn, " Design Methodologies for Advanced Flywheel Energy Storage", Dissertation to The Univerity of Texas at Austin, August 2013.

[7] M. A. Pichot and M. A. Driga, "Loss Reduction Strategies in Design of Magnetic Bearing Actuators for Vehicle Applications," IEEE Transactions on Magnetics, vol. 41, no. 1, pp. 492-496, Jan. 2005.

[8] A. A. Kordyuk, "Magnetic Levitation for Hard Superconductors," Journal of Applied Physics, vol. 83, pp. 610-612, 1998.

[9] J. R. Hull and A. Cansiz, "Vertical and Lateral Forces Between a Permanent Magnet and a High Temperature Superconductor," Journal of Applied Physics, vol. 86, no. 11, pp. 6396-6404, 1999.

[10] F. Grilli, et al. Finite-Element Method Modeling of Superconductors: From 2-D to 3-D. IEEE Trans. Appl. Supercond., vol. 15, no. 1, pp. 17-25, March 2005.

[11] C.S. Hearn, S.B. Pratap, D. Chen, and R.G. Longoria, "Reduced Order Dynamic Model of Permanent Magnet and HTSC Interaction in an Axisymmetric Frame," IEEE Transactions on Mechatronics, in press, Aug. 2013.

[12] C.S. Hearn, S.B. Pratap, D. Chen, and R.G. Longoria, " Lumped Parameter Model to Describe Dynamic Translational Interaction for High Temperature Superconducting Bearings," IEEE Transactions on Applied Superconductivity, in press, Jan. 2014.

[13] Karnopp, Dean C., Margolis, Donald L., and Rosenberg, Ronald C. System Dynamics: Modeling and Simulation of Mechatronic Systems. 3rd Ed. John Wiley and Sons, New York, 2000.

[14] Smythe, William R., Static and Dynamic Electricity, Hemisphere Publishing, New York, 1989, pp. 234, 290-291

[15] M. Ikeda, A. Wongsatanawarid, H. Seki and M. Murakami, "Interaction of bulk superconductors with flywheel rings made of simple permanent magnets," Physica C, vol. 469, pp. 1270-1273, 2009.

[16] G. G. Sotelo, A. C. Ferreira and J. R. de Andrade, "Halbach Array Superconducting Magnetic Bearing for a Flywheel Energy Storage System," IEEE Transactions on Applied Superconductivity, vol. 15, no. 2, pp. 2253 - 2256, June 2005.

[17] F. N. Werfel, U. Floegel-Delor, R. Rothfeld, T. Riedel, B. Goebel, D. Wippich and P. Schirrmeister, Superconductor Bearings, Flywheels and Transportation, Superconductor Science and Technology, vol. 25, 014007 (16pp), 2012.

[18] G. Schweitzer, "Chapter 7: Dynamics of the Rigid Rotor," in *Magnetic Bearings; Theory, Design, and Application to Rotating Machinery*, Berlin, Springer-Verlag, 2009, pp. 167-189.